ChemBioChem

Research Article
doi.org/10.1002/cbic.202500457

Chemistry Europe
European Chemical Societies Publishing

www.chembiochem.org

Indomethacin-Naphthalimide-Based AIEgen for Illuminating Golgi Apparatus

Phanindra Kumar, Tripti Mishra, Sanyam, Asima Sahu, Anirban Mondal, and Sudipta Basu*

Golgi apparatus (GA) is a complex organelle controlling subcellular protein modifications, sorting, and transport. Dysregulation in GA leads to cancer development and metastasis. Consequently, development of small molecule fluorophores for illuminating GA in cancer cells remains a major challenge. To address this, herein, a small molecule library of four aggregation-induced emissive probes (AIEgens) is designed and synthesized, having (a) indomethacin, a nonsteroidal anti-inflammatory drug (NSAID) for GA homing; (b) 1,8-naphthalimide-N,N′-disubstituted aniline as AIE inducer; and (c) amide/ester linkage between NSAID and AIE inducer. All the library members exhibited excellent AIE property in THF/water binary solvent systems through self-assembly in water. Interestingly, one of the library members (compound 13), consisting of napthalimide-N,N′-dimethyl aniline as AIE inducer and amide linkage, efficiently homes into the GA of HCT-116 colon cancer cells within 30 min and self-assembled into 2D nanoscale materials, as shown by scanning electron and atomic force microscopy and confirmed by molecular dynamics (MD) simulations. Moreover, quantum mechanical calculations revealed intramolecular charge transfer (CT) between N,N′-dimethyl aniline (donor) and naphthalimide (acceptor) as the underlying mechanism of the photophysical properties of compound 13. This novel AIEgen can serve as a chemical biology tool to visualize GA in cancer cells for next-generation cancer therapeutics.

1. Introduction

The Golgi apparatus (GA) is a vital subcellular organelle that orchestrates key biological signaling pathways, including protein post-translational modification (PTM), sorting,and secretion.[1–6] Consequently, any dysregulation in the structure, function, or dynamics of the GA is closely associated with a range of pathological conditions, notably the development and progression of cancer.[7–12] In recent years, the visualization of GA structure and dynamics in both normal and cancerous cells has emerged as a promising approach in the field of cancer theranostics.[13,14] However, the development of novel small-molecule fluorophores specifically targeting the GA has remained a significant challenge, primarily due to a limited understanding of GA-specific homing mechanisms and biomarkers.

In this context, small-molecule fluorophores tagged with GA-targeting chemical moieties have been recently developed for effective GA imaging in cancer cells.[15] Among these, aggregation-induced emission (AIE)-based fluorophores (AIEgens) have gained considerable attention due to their unique tunable luminescence, high photostability, and resistance to photobleaching.[16–21] AIEgens have been extensively explored for imaging and perturbing various subcellular organelles—including mitochondria, endoplasmic reticulum (ER), lysosomes, and lipid droplets—in cancer cells, demonstrating their potential for bioimaging and theranostic applications.[22–29] Despite these advancements, the application of AIEgens for GA imaging has been limited, primarily due to the scarcity of suitable GA-targeting chemical entities.[30–36]

To overcome this limitation, we have designed and synthesized a small-molecule library comprising four compounds, incorporating the following key components: (a) indomethacin, a nonsteroidal anti-inflammatory drug (NSAID), chosen for its GA-homing capability via specific binding to cyclooxygenase-2 (COX-2)—an enzyme localized in the GA;[37] (b) a 1,8-naphthalimide core functionalized with an N,N′-disubstituted aniline moiety to induce AIE properties;[38] and (c) an amide or ester linkage to integrate the NSAID and AIEgen moieties.[39] This design allowed us to explore how variations in the N,N′-disubstituted aniline unit and linker type (amide versus ester) influence the photophysical behavior and GA targeting capabilities of the compounds. All members of the library demonstrated excellent AIE characteristics in THF/water and acetonitrile/water binary solvent systems, forming nanoscale self-assembled structures in aqueous media. Among the compounds, compound 13, featuring a 1,8-naphthalimide-N,N′-dimethylaniline scaffold linked via an amide bond to indomethacin, showed remarkable GA-targeting ability. Confocal microscopy revealed efficient localization of compound 13 within the GA of HCT-116 colon cancer cells within 30 min, with retention for up to 3 h, and only minimal off-target localization to lysosomes and ER. Additionally, the compound also homed into RPE-1 noncancerous cells within 3 h. Scanning electron microscopy (SEM) and atomic force microscopy (AFM) confirmed the formation of 2D nanoscale self-assembled structures

P. Kumar, T. Mishra, Sanyam, A. Sahu, A. Mondal, S. Basu
Department of Chemistry
Indian Institute of Technology (IIT) Gandhinagar
Palaj, Gandhinagar, Gujarat 382355, India
E-mail: sudipta.basu@iitgn.ac.in

Supporting information for this article is available on the WWW under https://doi.org/10.1002/cbic.202500457

of compound 13 in water, consistent with its AIE behavior. Quantum mechanical calculations indicated that an intramolecular charge transfer (ICT) between the electron-donating N,N′-dimethylaniline group and the electron-accepting naphthalimide core was responsible for its solvent-dependent photophysical properties. Furthermore, molecular dynamics (MD) simulations validated the self-assembly behavior of compound 13 into stable nanoscale structures in water, reinforcing its AIE characteristics. This study highlights the critical role of the N,N′-dimethyl aniline moiety and amide linkage in conferring both AIE and GA-targeting capabilities. We anticipate that this novel AIEgen will be a powerful tool to illuminate GA for cancer therapeutics.

2. Results and Discussion

We hypothesized to design small molecule AIEgen library for Golgi apparatus (GA) which consists of (a) indomethacin, a GA homing moiety; (b) 1,8-naphthalimide-N,N′-disubstituted aniline as AIE inducer; and (c) amide and ester linkage to connect indomethacin and AIE inducer with a linker (**Figure 1**a); we have chosen indomethacin, a nonsteroidal anti-inflammatory drug (NSAID) due to its ability to bind specifically with the cyclooxegenase-2 (Cox-2) enzyme localized in GA. We have chosen 1,8-naphthalimide-N,N′-disubstituted aniline moiety to induce AIE property into the molecules as well as to understand the effect of N,N′-substitution on AIE property and GA homing efficiency.

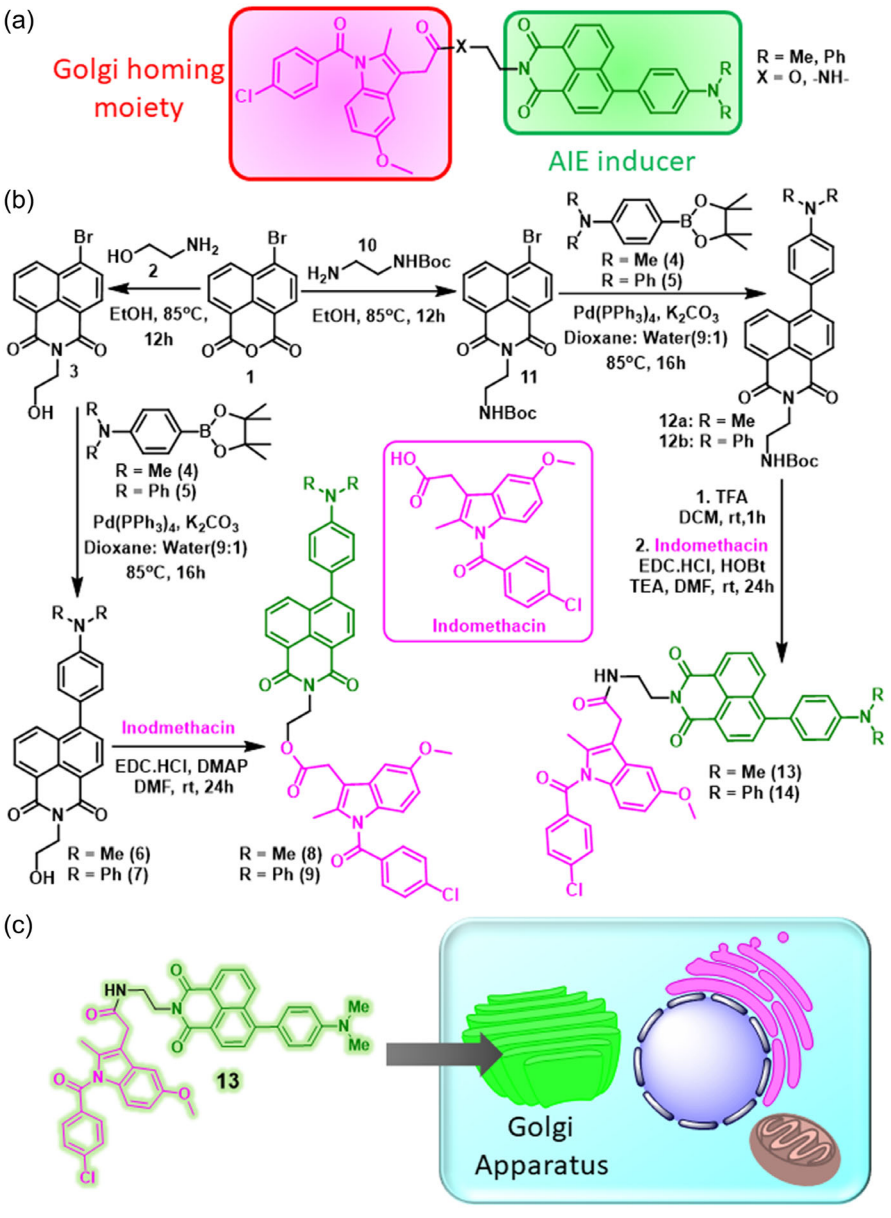

Figure 1. a) Design of the AIEgen library for Golgi apparatus (GA) imaging. b) Synthetic scheme of the GA targeted AIEgen library. c) Chemical structure of the lead molecule and mechanism of GA imaging.

Moreover, we anticipated that 1,8-naphthalimide having large planer π-conjugated systems, high fluorescence quantum yield, significant Stokes shift, thermal/photochemical stability, and functional tunability would augment the photophysical properties of our proposed AIEgens.[40,41] We have also chosen the amide and ester linkage to connect the NSAID and AIE inducer to verify the effect of linker functionality in efficient GA homing. Ester linkage is widely utilized to cleave the prodrug molecule due to their easy hydrolysis under physiological conditions, making them suitable for controlled release. On the other hand, amide linkers are more stable and offer longer circulation time along with driving the molecule in GA.[30,42] The synthesis of the proposed library was started by reacting 4-bromo-1,8-naphthalic anhydride (1) with ethanolamine (2) to obtain 6-bromo-2-(2-hydroxyethyl)-1H-benzo[*de*]isoquinoline-1,3(2H)-dione (3) which was further reacted with 4-(dimethylamino)phenylboronic acid pinacol ester (4) and 4-(diphenylamino)phenylboronic acid pinacol ester (5) in a Suzuki coupling reaction using $Pd(PPh_3)_4$ as catalyst to afford 6-(4-(dimethylamino)phenyl)-2-(2-hydroxyethyl)-1H-benzo[*de*] isoquinoline-1,3(2H)-dione (6) and 6-(4-(diphenylamino)phenyl)-2-(2-hydroxyethyl)-1H-benzo[*de*]isoquinoline-1,3(2H)-dione (7) respectively (Figure 1b). Finally compounds 6 and 7 were conjugated with indomethacin through ester linkage by using EDC.HCl and DMAP as coupling agents to obtain compound 8 and 9. On the other hand, 4-bromo-naphthalic anhydride (1) was refluxed with tert-butyl (2-aminoethyl) carbamate (10) in ethanol for 12 h to afford tert-butyl (2-(6-bromo-1,3-dioxo-1H-benzo[*de*]isoquinolin-2(3H)-yl)ethyl)carbamate (11) which was further derivatized using N,N-dimethyl-4-(4,4,5,5-tetramethyl-1,3,2-dioxaborolan-2-yl)aniline (4) and (4-(diphenylamino)phenyl)boronic acid (5) pinacol ester in Suzuki coupling condition using $Pd(PPh_3)_4$ as a catalyst to obtain 2-(2-aminoethyl)-6-(4-(dimethylamino)phenyl)-1H-benzo[*de*]isoquinoline-1,3(2H)-dione (12a) and 2-(2-aminoethyl)-6-(4-(diphenylamino)phenyl)-1H-benzo[*de*]isoquinoline-1,3 (2H)-dione (12b) respectively. The Boc-protection was removed from 12a and 12b by trifluoroacetic acid (TFA) followed by conjugating indomethacin through amide linkage using EDC.HCl/HOBt as coupling agents to obtain compounds 14 and 15. All the intermediates and final compounds were characterized by ^1H, ^{13}C NMR spectroscopy and HR-MS (Figure S1–S24, Supporting Information).

We further evaluated the photophysical properties of compounds 8, 9, 13, and 14. We measured the UV-Vis specta in different solvents like 1,4-dioxane, THF, acetonitrile, methanol, DMSO, and water which showed that all four molecules absorbed at $\lambda_{max} = 417–437$ nm (Figure S25, Supporting Information). It was noted that λ_{max} was red-shifted for compounds 8, 13, and 14 in water as well as the spectra became broader with reduced absorbance compared to the other organic solvents indicating a potential aggregation in water. Moreover, for compound 9, the absorbance increased in water along with red shift of λ_{max} (Figure S25b, Supporting Information). We also evaluated the fluorescence emission spectra of all the four compounds (8, 9, 13, and 14) in water, DMSO, methanol, acetonitrile, THF, and 1,4-dioxane. All four molecules showed fluorescence emission quenching in DMSO, methanol, and acetonitrile. However, all molecules showed significant fluorescence emission at $\lambda_{em} = 586–622$ nm in water and THF (Figure S26, Supporting Information) indicating potential restriction in intramolecular motion.

Interestingly, we observed a pronounced emission quenching for compounds 13 and 14, in comparison to 8 and 9 in water (Figure S26, Supporting Information), which can be attributed to the presence of amide linkers. Amide groups are well known to facilitate fluorescence quenching in aromatic or π-conjugated systems, particularly in polar solvents such as water. Acting as electron-withdrawing moieties, amide linkers can engage in nonradiative deactivation pathways—most notably photoinduced electron transfer (PET) and internal conversion—especially when they are conjugated with or positioned near the emissive core. The quenching efficiency of amides is highly solvent-dependent. In aqueous environments, the polarity and hydrogen-bonding capability of water can further stabilize charge-separated or nonemissive states. This stabilization lowers the energy barrier for charge transfer from the excited state of the chromophore to the amide group, enhancing the likelihood of nonradiative decay and thus reducing emission intensity.[43–45] To further substantiate this hypothesis, we performed nonradiative decay rate calculations (for the $S_1 \rightarrow S_0$ transition) for representative molecules: compound 9 (bearing an ester linker) and compound 14 (bearing an amide linker) using the ORCA quantum chemistry package at the B3LYP-D3BJ/6-31+G(d,p) level of theory, employing the CPCM solvation model for water. The calculated nonradiative decay rate for compound 9 was $2.45 \times 10^{10}\ s^{-1}$, whereas for compound 14, the rate was significantly higher at $8.40 \times 10^{10}\ s^{-1}$. This marked increase in the nonradiative decay rate for the amide-containing system supports the enhanced quenching observed experimentally. Furthermore, due to the stronger electron-donating capability of N,N-dimethylphenylamine moiety compared to triphenylamine, compounds 8 and 13 showed more red shifted fluorescence emission at $\lambda_{em} = 612$ and 622 nm respectively compared to the $\lambda_{em} = 590$ and 603 nm respectively for compound 9 and 14 (Figure S27, Supporting Information). All four compounds showed remarkable fluorescence emission at $\lambda_{em} = 552–581$ nm in 1,4-dioxane indicating the restriction in molecular motion in highly viscous solvent (Figure S28, Supporting Information).

We validated our hypothesis that compounds 8, 9, 13, and 14 would show AIE activity. We checked the emission behavior of all four compounds in THF/water binary solvent systems. All four compounds showed little fluorescence emission in 100% THF. However, when the water fraction was increased, the fluorescence emission was completely quenched until THF: water = 40:60 (v/v) for compounds 9, 13, and 14 and until THF: water = 30:70 (v/v) for compound 8 (**Figure 2**a–h and Figure S29, Supporting Information). However, a sharp increase in the fluorescence intensity was observed for all the compounds till 100% water. We further checked the AIE property of all four compounds (8, 9, 13, and 14) in acetonitrile/water binary solvent system. None of the compounds showed fluorescence emission in 100% acetonitrile, as well as until acetonitrile: water = 50:50 (v/v). However, all four molecules demonstrated increased fluorescence intensity in acetonitrile: water = 30:70 (v/v) till 100% water (Figure S30–S33, Supporting Information). We also measured the

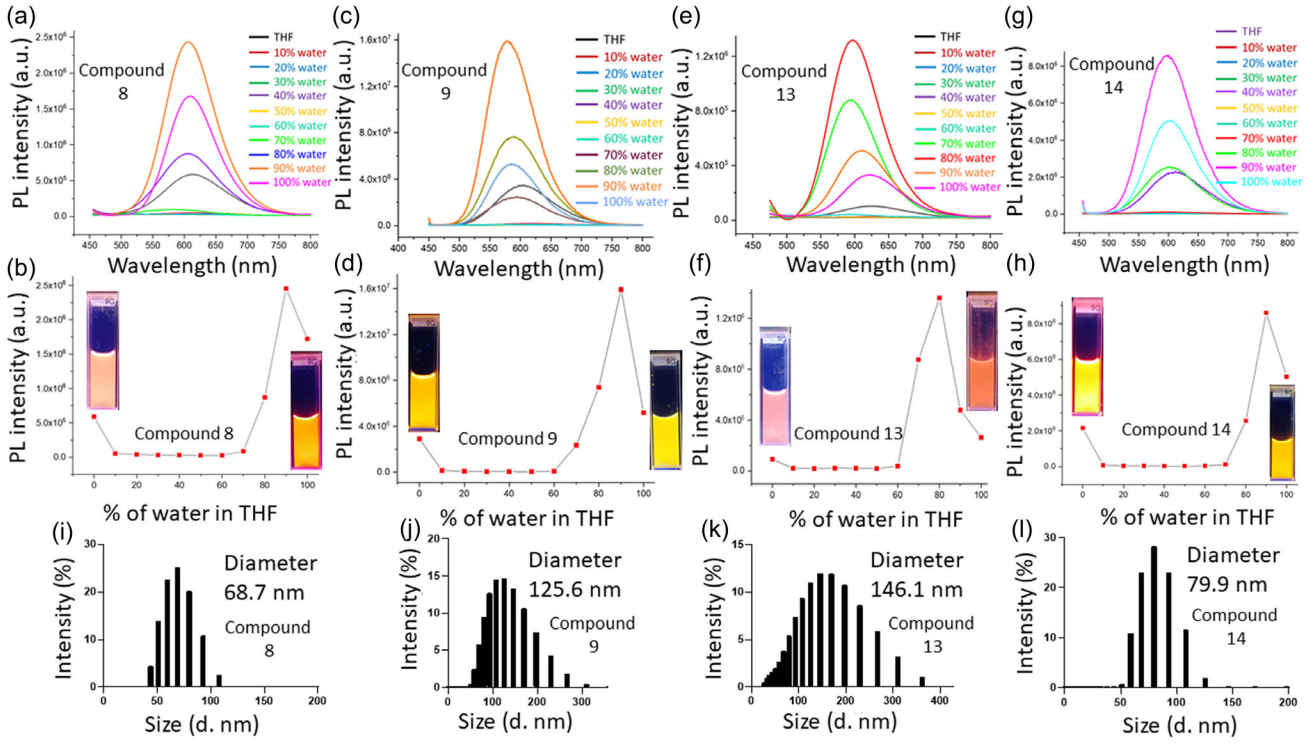

Figure 2. a,c,e,g) Change in fluorescence emission spectra of compounds 8, 9, 13, and 14 respectively in different THF/water ratio. b,d,f,h) Fluorescence emission intensity versus water fraction graph of compounds 8, 9, 13, and 14 respectively. i–l) Hydrodynamic diameter of compounds 8, 9, 13, and 14 in water from DLS.

fluorescence lifetime in THF, 80–90% water in THF, and 100% water for all four compounds. Interestingly, compound 9 showed high fluorescence lifetime of 17.9 and 16.3 ns at 90% water in THF and 100% water respectively (Figure S34, Table S1, Supporting Information). We also calculated the fluorescence quantum yield (QY) of all the four compounds in 100% water which showed 3.25%, 8.2%, 1%, and 4.5% QY for compounds 8, 9, 13, and 14, respectively (Table S2, Supporting Information). This fluorescence spectroscopy-based solvent titration confirmed that all four compounds showed AIE properties in THF/water and acetonitrile/water binary systems.

To confirm the aggregation formation, we suspended all four compounds in water and measured the size through dynamic light scattering (DLS). The hydrodynamic diameter was measured to be 68.7, 125.6, 146.1 and 79.9 nm for compound 8, 9, 13 and 14 respectively (Figure 2i–l). We further evaluated the aggregation formation by the Tyndall effect which clearly confirmed that all the compounds aggregated in 80–90% water in THF, 80–90% water in acetonitrile, and in 100% water, but no aggregation was found in DMSO, methanol, acetonitrile, THF, and 1,4-dioxane (Figure S35, Supporting Information). These DLS and Tyndall effect confirmed that all four compounds aggregated in water to show AIE activities.

As all the library members (8, 9, 13, and 14) showed AIE activity in water as hypothesized, we assessed their GA homing ability in HCT-116 colon cancer cells. We treated HCT-116 cells with compounds 9 and 14 for 3 h and observed the cells under confocal microscopy. Interestingly, we observed no fluorescence signal inside the cells which confirmed that compounds 9 and 14 could not enter the cells (Figure S36, Supporting Information). We further treated HCT-116 cells with compound 8 for 1 h and stained the GA with GA Tracker Red dye followed by visualization of the live cells under confocal microscopy. The confocal images showed that compound 8 entered the cells and exhibited merged yellow fluorescence signal by homing into GA with modest Pearson's correlation coefficient (PCC) = 0.67 (**Figure 3**a and Figure S37, Supporting Information). Finally, we treated HCT-116 cells with compound 13 in a time-dependent manner for 30 min and 1 and 3 h and stained the GA with GA Tracker Red dye. We visualized the cells under confocal microscopy which showed that compound 13 homed into the GA efficiently to produce bright merged yellow fluorescence signals with high PCC = 0.85, 0.82, and 0.83 at 30 min and 1 and 3 h respectively (Figure 3b and Figure S38, Supporting Information). We anticipated that compound 13 having dimethylphenylamine moiety was less hydrophobic compared to compound 9 and 14 having triphenylamine moiety, leading to its successful internalization into the cells.

We further evaluated the cross homing of compound 13 in other organelles like lysosomes and endoplasmic reticulum (ER). We treated HCT-116 cells with compound 13 for 1 h followed by staining the lysosomes and GA with LysoTracker Red and GA Tracker Red dye respectively. The confocal images of the live cells showed that compound 13 marginally internalized into lysosomes with low PCC = 0.65 (**Figure 4**a and Figure S39a, Supporting Information). On the other hand, we visualized that

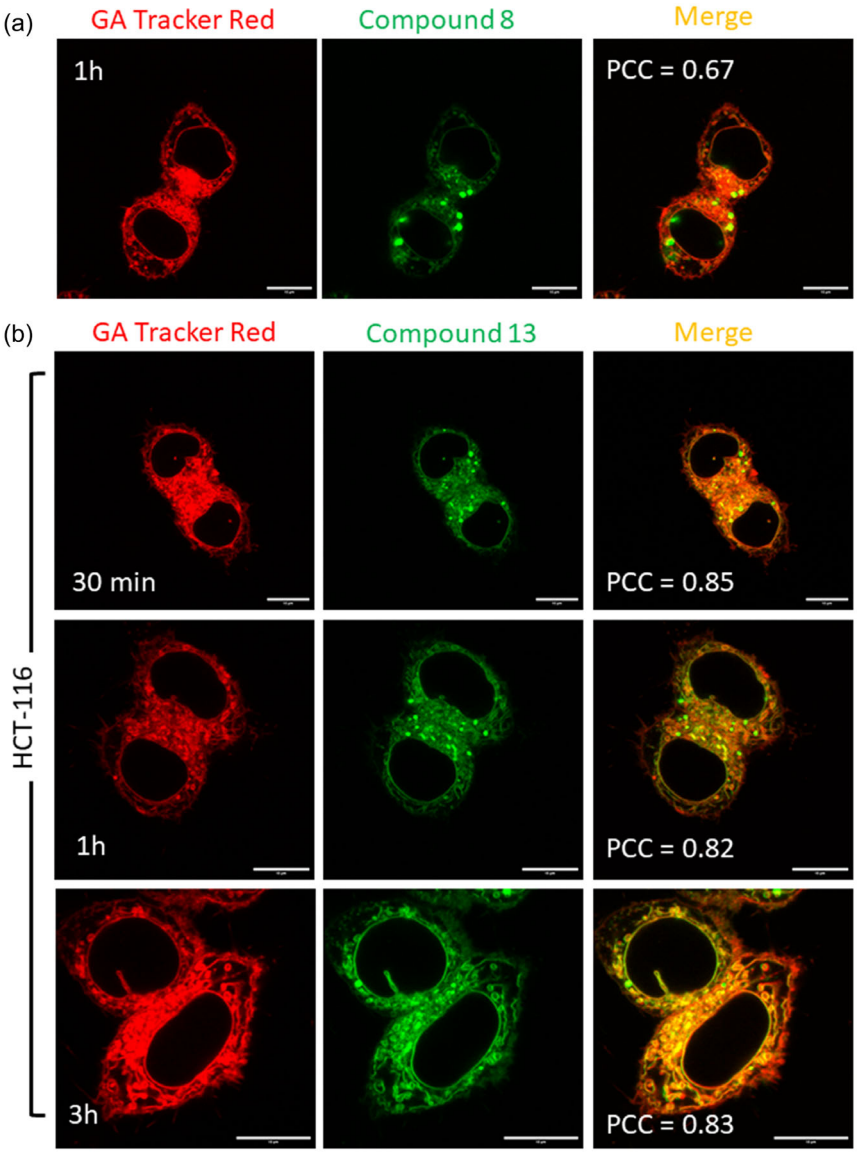

Figure 3. a) Confocal images of HCT-116 cells incubated with compound 8 for 1 h followed by staining the GA with GA Tracker Red dye. b) Confocal images of HCT-116 cells incubated with compound 13 for 30 min and 1 and 3 h, followed by staining GA with GA Tracker Red dye. Scale bar = 10 μm.

compound 13 homed into the ER modestly with PCC = 0.77 (Figure 4c and Figure S39b, Supporting Information), which was quite low from our previous observations.[36] We anticipated that compound 13 homed into the ER due to the effect of retrograde signaling and cross-talk between GA and ER.[46–48] We also evaluated the GA imaging capability of compound 13 in noncancerous RPE-1 human retinal pigment epithelial cells. We incubated RPE-1 cells with compound 13 for 3 h, stained GA with GA Tracker Red dye, and visualized the cells under confocal microscopy, which exhibited that compound 13 homed into the GA with PCC = 0.79 (Figure 4c and Figure S40, Supporting Information).

Furthermore, we checked the cytotoxicity of all the library members in HCT-116 cells. We incubated HCT-116 cells with all the library members (8, 9, 13, and 14) in a dose-dependent manner for 24 h and measured the cell viability by MTT assay. From the MTT assay, it was evident that compound 8, 9, and 14 showed no toxicity to the HCT-116 cells even in 30 μM concentration (Figure S41a, Supporting Information). However, interestingly, compound 13 showed 50% cell killing even at 1.25 μM concentration. We expected that compound 9 and 14 showed no toxicity in HCT-116 cells due to their inability to internalize into the cells. On the other hand, we anticipate that compound 13 homed into the GA and bound and inhibited Cox-2 in GA leading to the modest toxicity in HCT-116 cells. We also evaluated the cytotoxicity of compound 13 in RPE-1 cells in a dose-dependent manner at 24 h post-incubation, which revealed that compound 13 was nontoxic even at 30 μM concentration (Figure S41b, Supporting Information). Hence, compound 13 could be further explored as theranostic probe to understand the role of NSAIDs in the chemical biology of GA toward cancer therapy. These confocal microscopy images clearly confirmed that among all the

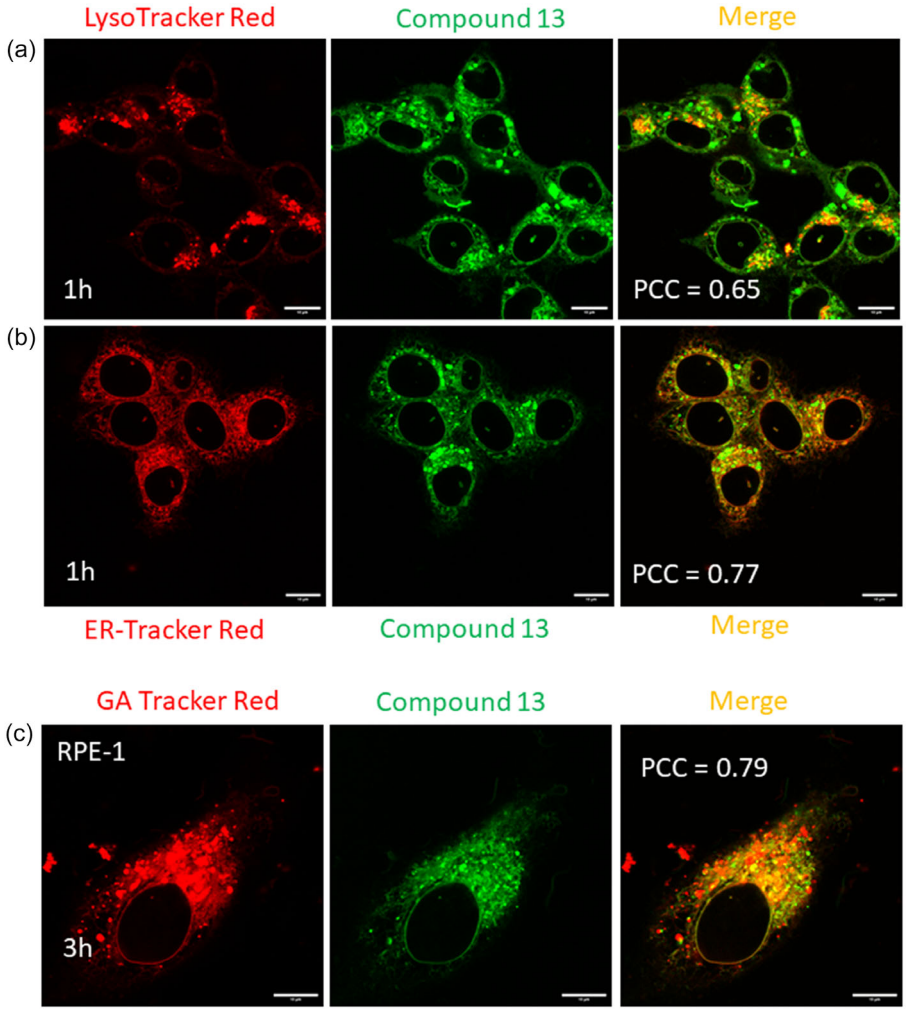

Figure 4. a,b) Confocal images of HCT-116 cells incubated with compound 13 for 1 h, followed by staining lysosomes and ER by LysoTracker Red and ER Tracker Red dyes respectively. c) Confocal images of RPE-1 cells incubated with compound 13 for 3 h followed by staining the GA with GA Tracker Red dye. Scale bar = 10 μm.

library members, compound 13 internalized into the HCT-116 cells and efficiently illuminated GA by homing into it within 30 min, without much less cross homing into lysosomes and ER as well as showing moderate toxicity. Moreover, compound 13 also effectively illuminated the GA in noncancerous RPE-1 cells within 3 h.

We further analyzed the GA homing ability of compound 13 in HeLa (cervical cancer), A549 (lung cancer) and COS-7 (noncancerous kidney fibroblast) cells as the Cox-2 expressions are much higher in HeLa and A549 cells compared to COS-7 cells.[49,50] We incubated HeLa, A549, and COS-7 cells with compound 13 for 30 min and 1 h, followed by staining GA by GA Tracker Red dye, and visualized the cells under confocal microscopy. The confocal images showed that compound 13 homed into the GA of HeLa cells with PCC = 0.5 and 0.65 at 30 min and 1 h respectively (**Figure 5**a and Figure S42, Supporting Information). On the other hand, compound 13 homed into the GA of A549 cell much efficiently with PCC = 0.7 and 0.75 at 30 min and 1 h respectively (Figure 5b, S43, Supporting Information). In contrast, in COS-7 cells, compound 13 localized into the GA marginally with PCC = 0.41 and 0.48 respectively at 30 min and 1 h (Figure 5c and Figure S44, Supporting Information). These confocal images confirmed that based on the higher Cox-2 expressions in the cancer cells, compound 13 homed into HCT-116 cells much efficiently compared to A549 and HeLa cells. On the other hand, due to the reduced Cox-2 expression into the noncancerous cells, compound 13 homed into the GA less effectively in COS-7 cells.

As we have found out compound 13 as the promising AIEgen for GA imaging in HCT-116 cells, we further validated the photophysical property of compound 13 by quantum mechanical calculations using the ORCA 5.0.3 software package.[51] The geometry of compound 13 in its electronic ground state was optimized at the B3LYP/def2-SVP level of theory. Moreover, excited-state optimizations were performed to estimate the emission wavelengths in various solvents: water, acetonitrile (MeCN), and THF. Solvent effects were incorporated through the conductor-like polarizable continuum model (CPCM). To further understand the nature of the excited states, an exciton analysis was

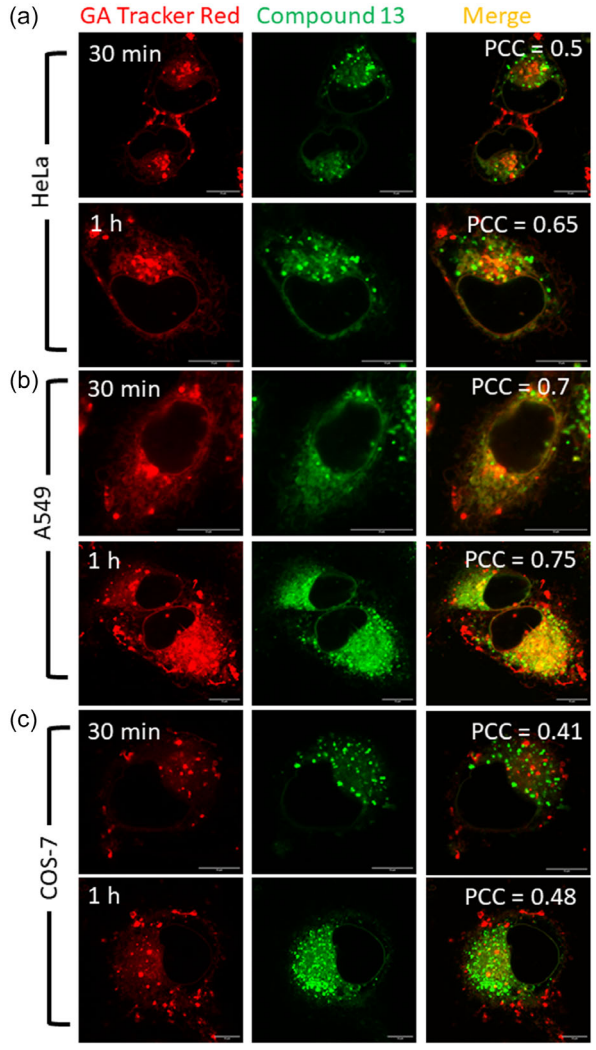

Figure 5. Confocal images of a) HeLa, b) A549, and c) COS-7 cells incubated with compound 13 for 30 min and 1 h, followed by staining the GA with GA Tracker Red dye. Scale bar = 10 μm.

conducted within ORCA to distinguish between charge–transfer (CT) and locally excited (LE) characters. From these quantum mechanical calculations, it was found that compound 13 exhibited emission in the red spectral region, with the emission wavelength ranging from 647.5 to 672.2 nm in water, MeCN, and THF which have a decreasing polarity trend: H_2O > MeCN > THF (Table S3, Supporting Information). Analysis of the charge–transfer (CT) characteristics, confirms the polar nature of the molecule, characterized by a permanent dipole moment. The charge density difference map revealed a unidirectional charge transfer from the donor region (depicted in blue) to the acceptor region (in yellow), reinforcing the CT character (**Figure 6**a). The computed charge transfer number of 0.967, close to the ideal value of 1, further supported the strong CT nature of the excited state. Additionally, Figure 6a showed clear spatial separation between donor and acceptor moieties, resulting in negligible singlet–triplet energy splitting. Among the solvents studied, THF, being the least polar, provided limited stabilization of the polar excited singlet state (S_1) due to weaker solvent–solute interactions. Consequently, the S_1 energy was highest in THF. In contrast, water (H_2O), the most polar solvent, provided the greatest stabilization through favorable polar–polar interactions. Acetonitrile (MeCN), with intermediate polarity, resulted in moderate stabilization of the S_1 state. A distinct bathochromic shift (red shift) in emission wavelength was observed along the solvent polarity gradient (THF → MeCN → H_2O), reflecting progressive stabilization of the CT-excited state. This solvent-dependent stabilization also influenced the oscillator strength (f): in THF, where CT stabilization was minimal, the oscillator strength was higher ($f = 0.0005$), indicating a greater likelihood of radiative transition. In contrast, in MeCN and H_2O, where CT stabilization was stronger, the oscillator strength decreased to $f = 0.0002$, consistent with reduced radiative probability associated with enhanced CT character.

To validate the aggregation of compound 13 to show AIE property, we visualized the self-assembly in water and THF: water = 20:80 (v/v) through SEM and AFM. The SEM and AFM images showed that compound 13 self-assembled into 2D nano-materials in both 100% water as well as THF: water = 20:80 (v/v) (Figure 6b–e and Figure S45, S46, Supporting Information). These SEM and AFM images confirmed that compound 13 showed AIE property by self-assembly into nanoscale morphologies. We further validated the aggregation behavior of compound 13 by molecular dynamics (MD) simulations. The aggregation behavior of compound 13 in solution was explored using molecular dynamics (MD) simulations implemented in the GROMACS package.[52,53] A single solute molecule was initially solvated with 1000 water molecules in a simulation box. This configuration was replicated along all three Cartesian axes to yield a system containing 8 solute molecules and 8000 solvent molecules. The starting configurations (or packing) and the final morphologies of the system are shown in Figure 6f–i. As shown in Figure 6f, the molecules were initially spaced apart, representing the general packing structure observed in all solvents (THF, MeCN, and water). Figure 6g–i illustrate the final configurations in THF, MeCN, and H_2O. In Figure 6g, the molecules remained well-separated even in the final configuration, consistent with the behavior observed in THF. In contrast, Figure 6h for MeCN shows a greater degree of aggregation than THF, although the level of aggregation was still minimal compared to the case in water. Figure 6i demonstrates that, in water, the molecules exhibit substantial aggregation, with some molecules even forming a pentamer out of the eight total molecules. Thus, the degree of aggregation was most significant in water, followed by MeCN, and least in THF. To further quantify this aggregation, we plotted the radial distribution function, which indicated the probability of finding a molecule in the vicinity of a reference molecule. The provided RDF represented the center-of-mass to center-of-mass distribution of the organic molecule across different solvents. Figure 6j shows the highest probability of finding an organic molecule in proximity to another (see peak height) in water, with the distance between molecules being notably shorter (only 5 Å). In the case of MeCN, the probability of finding neighboring molecules was lower, as evidenced by the reduced peak heights and the shift

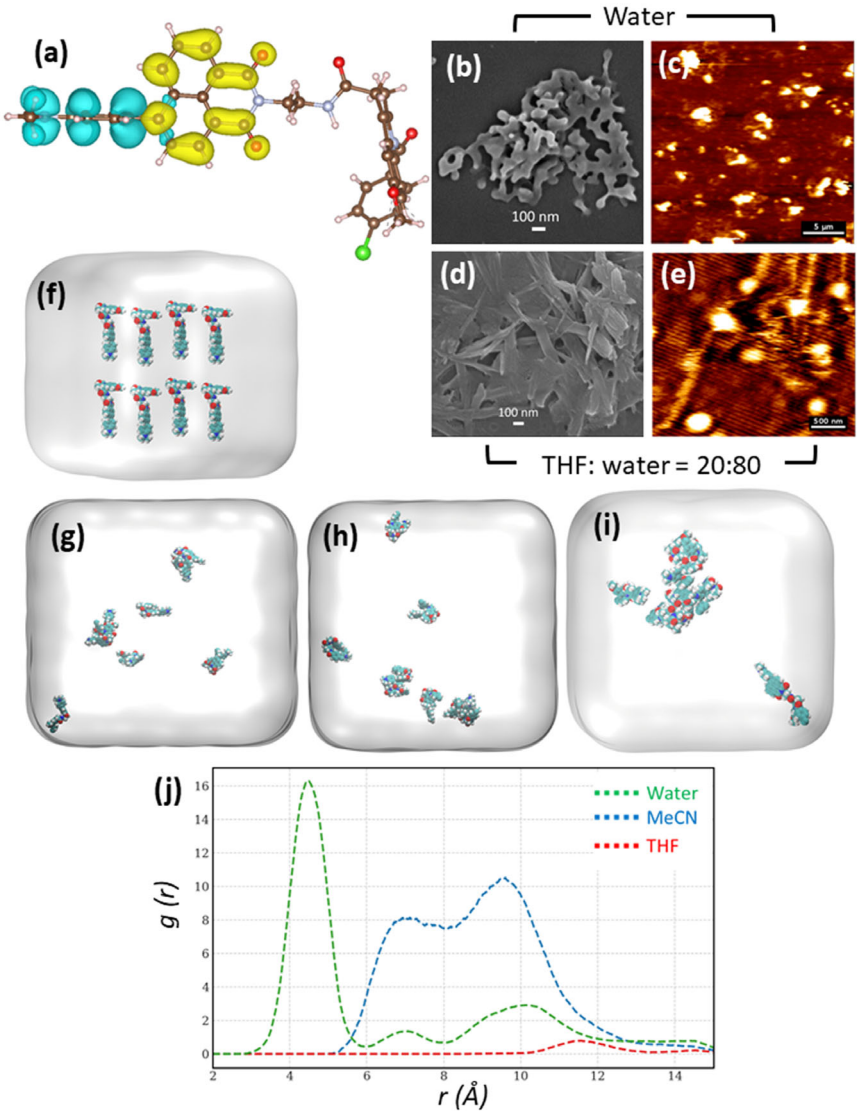

Figure 6. a) The charge transfer density difference plot of the compound 13 illustrates the unidirectional charge transfer from the donor (blue) to the acceptor (yellow) regions. It highlights the molecule's charge transfer characteristics. b,c) FESEM and AFM images of self-assembled nano-structures formed from compound 13 in water. d,e) FESEM and AFM images of self-assembled nanostructures formed from compound 13 in THF: water = 20:80. f) Initial configuration of the packed compound 13; g) final configuration of compound 13 in THF; h) final configuration of compound 13 in MeCN; i) final configuration of compound 13 in water from MD simulation. j) Radial distribution function (RDF) plots showing the aggregation behavior of the organic molecule from center of mass to center of mass in different solvents.

to larger intermolecular distances (two peaks at 7 and 9 Å). This indicated that molecules in MeCN were less likely to aggregate than those in water. THF showed the lowest probability of molecular proximity, with the peak height approaching unity, indicating a minimal likelihood of aggregation, and the intermolecular distances were comparatively larger than in both waterand MeCN.

3. Conclusion

In conclusion, we have designed and synthesized a small molecule AIEgen library of four compounds having indomethacin as GA homing moiety, 1,8-naphthalimide-N,N′-disubstituted aniline as AIE inducer and amide/ester linkage to connect the GA homing moiety and the AIE inducer. All the library members showed AIE activity in THF/water and acetonitrile/water binary solvent through self-assembly promoted aggregation. Interestingly, one of the library members (compound 13) consisting amide linkage and 1,8-naphthalimide-N,N′-dimethyl aniline homed into the GA of HCT-116 colon cancer cell within 30 min in remarkably efficient manner compared to other library members. Compound 13 self-assembled into 2D nanoscale structures observed by FESEM and AFM studies and further confirmed by MD simulations. Moreover, quantum mechanical calculations confirmed that intramolecular charge transfer (CT) between N,N′-dimethyl aniline (donor) and naphthalimide (acceptor) moieties was responsible for the unique photophysical properties of compound 13. We anticipate that N,N′-dimethyl aniline and amide linkages are

necessary for designing AIEgens for imaging GA and compound 13 can be a useful tool to understand the chemical biology to visualize and impair GA for cancer theranostic applications.

Supporting Information

The authors have cited additional references within the Supporting Information.[55–60]

Acknowledgements

P.K. and T.M. contributed equally to this work. S.B. acknowledges IIT Gandhinagar, Gujarat Council on Science and Technology (GUJCOST/STI/R&D/2020-21/1302) and Science and Engineering Research Board (CRG/2020/001127) for funding. P.K. and Sanyam acknowledge CSIR-UGC-JRF for doctoral fellowship. Sanyam and A.M. thank PARAM Ananta for computational resources. A.S. thanks DST-INSPIRE fellowship for her doctoral research (DST/INSPIRE Fellowship/[IF210167]).

Conflict of Interest

The authors declare no conflict of interest.

Data Availability Statement

The data that support the findings of this study are available in the supplementary material of this article.

Keywords: AIEgen · Golgi apparatus · indomethacin · molecular dynamics simulation · self-assembly

[1] J. R. Baker, *Nature* **1951**, *168*, 1089.
[2] C. Featherstone, *Science* **1998**, *282*, 2172.
[3] J. Li, E. Ahat, Y. Wang, *Results Probl. Cell Differ.* **2019**, *67*, 441.
[4] F. Zappa, M. Failli, M. A. De Matteis, *Curr. Opin. Cell Biol.* **2018**, *50*, 102.
[5] A. Eisenberg-Lerner, R. Benyair, N. Hizkiahou, N. Nudel, R. Maor, M. P. Kramer, M. D. Shmueli, I. Zigdon, M. C. Lev, A. Ulman, J. Y. Sagiv, M. Dayan, B. Dassa, M. Rosenwald, I. Shachar, J. Li, Y. Wang, N. Dezorella, S. Khan, Z. Porat, E. Shimoni, O. Avinoam, Y. Merbl, *Nat. Commun.* **2020**, *11*, 409.
[6] J. Gao, A. Gao, H. Zhou, L. Chen, *Cell Biol. Int.* **2022**, *46*, 1309.
[7] S. Bui, I. Mejia, B. Díaz, Y. Wang, *Front. Cell Dev. Biol.* **2021**, *9*, 806482.
[8] R. Bajaj, A. N. Warner, J. F. Fradette, D. L. Gibbons, *Cells* **2022**, *11*, 1484.
[9] J. Liu, Y. Huang, T. Li, Z. Jiang, L. Zeng, Z. Hu, *Int. J. Mol. Med.* **2021**, *47*, 38.
[10] Y. Li, L. Mu, Y. Li, Y. Mi, Y. Hu, X. Li, D. Tao, J. Qin, *Cell Death Dis.* **2024**, *15*, 417.
[11] M. Martins, A. S. Fernandes, N. Saraiva, *Int. J. Biochem. Cell Biol.* **2022**, *145*, 106174.
[12] M. Martins, J. Vieira, C. Pereira-Leite, N. Saraiva, A. S. Fernandes, *Biology* **2024**, *13*, 1.
[13] C. Preisinger, B. Short, V. De Corte, E. Bruyneel, A. Haas, R. Kopajtich, J. Gettemans, F. A. Barr, *J. Cell Biol.* **2004**, *164*, 1009.
[14] L. Lu, Q. Zhou, Z. Chen, L. Chen, *J. Cell. Physiol.* **2018**, *233*, 2911.
[15] S. Xu, K. C. Yan, Z. H. Xu, Y. Wang, T. D. James, *Chem. Soc. Rev.* **2024**, *53*, 7590.
[16] J. Mei, N. L. C. Leung, R. T. K. Kwok, J. W. Y. Lam, B. Z. Tang, *Chem. Rev.* **2015**, *115*, 11718.
[17] B. Liu, R. Zhang, *Faraday Discuss.* **2017**, *196*, 461.
[18] X. Jiang, H. Gao, X. Zhang, J. Pang, Y. Li, K. Li, Y. Wu, S. Li, J. Zhu, Y. Wei, L. Jiang, *Nat. Commun.* **2018**, *9*, 3799.
[19] S. Wang, K. Zhou, X. Lyu, H. Li, Z. Qiu, Z. Zhao, B. Z. Tang, *Chem. Biomed. Imaging* **2023**, *1*, 509.
[20] P. Cen, J. Huang, C. Jin, J. Wang, Y. Wei, H. Zhang, M. Tian, *Aggregate* **2023**, *4*, e352.
[21] J. Li, Z. Zhuang, X. Lou, Z. Zhao, B. Z. Tang, *Chem. Biomed. Imaging* **2023**, *1*, 785.
[22] F. Hu, B. Liu, *Org. Biomol. Chem.* **2016**, *14*, 9931.
[23] J. Qian, B. Z. Tang, *Chem* **2017**, *3*, 56.
[24] Y. Cai, C. Gui, K. Samedov, H. Su, X. Gu, S. Li, W. Luo, H. H. Y. Sung, J. W. Y. Lam, R. T. K. Kwok, I. D. Williams, A. Qin, B. Z. Tang, *Chem. Sci.* **2017**, *8*, 7593.
[25] Y. Li, Y. Wu, J. Chang, M. Chen, R. Liu, F. Li, *Chem. Commun.* **2013**, *49*, 11335.
[26] S. Patil, S. Pandey, A. Singh, M. Radhakrishna, S. Basu, *Chem. Eur. J.* **2019**, *25*, 8229.
[27] J. Ingle, B. Das, K. Chaudhary, A. Mondal, S. Basu, *ChemBioChem* **2023**, *24*, e202300379.
[28] J. Ingle, H. Dedaniya, C. Mayya, A. Mondal, D. Bhatia, S. Basu, *Chem. Eur. J.* **2022**, *28*, e202200203.
[29] X.–Z. Yang, S. Yao, J. Wu, J. Diao, W. He, Z. Guo, Y. Chen, *Smart Mol.* **2024**, *2*, e20240040.
[30] X. Wang, X. Wang, Y. Li, Z. Qi, *Dyes Pigm.* **2024**, *222*, 111897.
[31] M. Liu, Y. Chen, Y. Guo, H. Yuan, T. Cui, S. Yao, S. Jin, H. Fan, C. Wang, R. Xie, W. He, Z. Guo, *Nat. Commun.* **2022**, *13*, 2179.
[32] P. Xiao, K. Ma, M. Kang, L. Huang, Q. Wu, N. Song, J. Ge, D. Li, J. Dong, L. Wang, D. Wang, B. Z. Tang, *Chem. Sci.* **2021**, *12*, 13949.
[33] Y. Luo, S. Zhang, H. Wang, Q. Luo, Z. Xie, B. Xu, W. Tian, *CCS Chem.* **2022**, *4*, 456.
[34] M. Yuan, J. Hu, W. H. Chen, *Org. Biomol. Chem.* **2023**, *21*, 5732.
[35] S. Li, K. Yang, J. Zeng, Y. Ding, D. Cheng, L. He, *ACS Omega* **2022**, *7*, 9929.
[36] P. Kumar, T. Mishra, A. M. Sanyam, S. Basu, *ACS Appl. Bio Mater.* **2025**, *8*, 1524.
[37] H. Zhang, J. Fan, J. Wang, S. Zhang, B. Dou, X. Peng, *J. Am. Chem. Soc.* **2013**, *135*, 11663.
[38] A. F. Henwood, N. Curtin, S. Estalayo-Adrián, A. J. Savyasachi, T. A. Gudmundsson, J. I. Lovitt, L. C. Sigurvinsson, H. L. Dalton, C. S. Hawes, D. Jacquemin, D. F. O'Shea, T. Gunnlaugsson, *Chem* **2024**, *10*, 578.
[39] X. C. Feng, G. Zhang, R. Sun, Y. J. Xu, J. F. Ge, *Dyes Pigm.* **2022**, *208*, 110796.
[40] X. Lv, X. Luo, Y. Bao, Y. Qu, X. Zhang, F. Liu, J. Sun, *J. Photochem. Photobiol. A* **2025**, *459*, 116002.
[41] X. Luo, Y. Qu, Y. Zhang, Y. Wu, W. Yuan, L. Wang, *Chem. Eng. J.* **2021**, *415*, 129095.
[42] X.-C. Feng, G. Zhang, R. Sun, Y.-J. Xu, J.-F. Ge, *Dyes Pigm.* **2023**, *208*, 111040.
[43] P. M. Froehlich, K. Nelson, *J. Phys. Chem.* **1978**, *82*, 2401.
[44] P. L. Muño, P. R. Callis, *J. Phys. Chem. B* **2009**, *113*, 2572.
[45] E. M. Espinoza, J. A. Clark, J. B. Derr, D. Bao, B. Georgieva, F. H. Quina, V. I. Vullev, *ACS Omega* **2018**, *3*, 12857.
[46] H. Zhang, M. Rui, Z. Ma, S. Gong, S. Zhang, Q. Zhou, C. Gan, W. Gong, S. Wang, *iScience* **2024**, *27*, 108545.
[47] A. Spang, *Cold Spring Harb. Perspect. Biol.* **2013**, *5*, a013391.
[48] D. Wlodkowic, J. Skommer, D. McGuinness, C. Hillier, Z. Darzynkiewicz, *Leuk. Res.* **2009**, *33*, 1440.
[49] D. K. Petkova, C. Clelland, J. Ronan, L. Pang, J. M. Coulson, S. Lewis, A. J. Knox, *Respir. Med.* **2004**, *98*, 164.
[50] H. Zhang, J. Fan, J. Wang, S. Zhang, B. Dou, X. Peng, *J. Am. Chem. Soc.* **2013**, *135*, 11663.
[51] F. Neese, *WIREs Comput. Mol. Sci.* **2012**, *2*, 73.
[52] B. Hess, C. Kutzner, D. Van Der Spoel, E. Lindahl, *J. Chem. Theory Comput.* **2008**, *4*, 435.
[53] S. Pronk, S. Páll, R. Schulz, P. Larsson, P. Bjelkmar, R. Apostolov, M. R. Shirts, J. C. Smith, P. M. Kasson, D. van der Spoel, B. Hess, E. Lindahl, *Bioinformatics* **2013**, *29*, 845.

Manuscript received: June 9, 2025
Revised manuscript received: July 29, 2025
Version of record online: